On the Self-Assembly of Brush Block Copolymers in Thin Films

Sung Woo Hong,[†,‡,§] Weiyin Gu,[†,§] June Huh,[∥] Benjamin R. Sveinbjornsson,[⊥] Gajin Jeong,[§] Robert Howard Grubbs,[⊥,*] and Thomas P. Russell[§,*]

[§]Department of Polymer Science and Engineering, University of Massachusetts Amherst, 120 Governors Drive, Amherst, Massachusetts 01003, United States, [∥]Department of Material Science and Engineering, Yonsei University, 134 Shinchon-dong, Seodaemun-gu, Seoul 120-749 Korea, and [⊥]Division of Chemistry and Chemical Engineering, California Institute of Technology, Pasadena, California 91125, United States. [‡]These authors contributed equally to this work (S.W.H. and W.G.). [†]Present address: Samsung Advanced Institute of Technology (SAIT), Mt. 14—1, Nongseo-dong, Giheung-gu, Yongin-si, Gyeonggi-do 446—712, Republic of Korea (S.W.H.).

ABSTRACT We describe a simple route to fabricate two dimensionally well-ordered, periodic nanopatterns using the self-assembly of brush block copolymers (brush BCPs). Well-developed lamellar microdomains oriented perpendicular to the substrate are achieved, without modification of the underlying substrates, and structures with feature sizes greater than 200 nm are generated due to the reduced degree of chain entanglements of brush BCPs. A near-perfect linear scaling law was found for the period, *L*, as a function of backbone degree of polymerization (DP) for two series of brush BCPs. The exponent increases slightly from 0.99 to 1.03 as the side chain molecular weight increases from ~2.4 to ~4.5 kg/mol^{-1} and saturated with further increase in the side chain molecular weight due to the entropic penalty associated with the packing of the side chains. Porous templates and scaffolds from brush BCP thin films are also obtained by selective etching of one component.

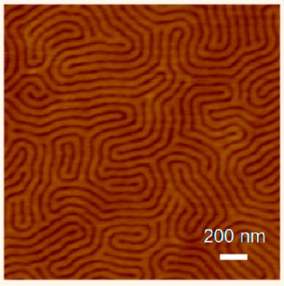

KEYWORDS: brush polymers · solvent-annealing · self-assembly · periodic nanopatterns · large feature sizes

Well-defined, periodic morphologies with features from the nanometer to hundreds of nanometer size scale have received considerable attention, because they can be used as templates and scaffolds for the fabrication of nanodots, nanowires, magnetic storage media, semiconductors, and optical devices, including polarizers and photonic band gap materials.[1−15] The self-assembly of block copolymers (BCPs) is proving to be one of the more promising bottom-up approaches to generate such morphologies in a cost-effective, robust, and scalable manner.[10,12,14,16−24] While there has been a tremendous drive to continually reduce the size scale of the features (with 3 nm feature sizes being the smallest achieved to date[21]), there are still numerous applications, as for example polarizers and photonic bandgap materials, that require feature sizes on the scale of hundreds of nanometers. The use of the self-assembly or directed self-assembly of BCPs could significantly reduce the number of steps required to generate features of this size and, therefore, lead to a substantial cost savings. Since the period (pitch) of BCP morphologies and the dimensions of microdomains scale approximately with the 2/3 power of the molecular weight (for BCPs comprised of flexible chains in the strong segregation limit), achieving large scale feature requires the use of exceptionally high molecular weight BCPs. There has not been much, if any, success in using high molecular weight (MW) BCPs to achieve large-scale features, because the diffusion of the polymers is exceptionally slow,[25] which significantly retards the self-assembly of the BCPs into highly ordered arrays of microdomains, as well as the elimination of defects in the resultant morphologies. Supercritical carbon dioxide (CO_2) at elevated temperatures has been used to swell BCPs, enhance the diffusion, and to order the BCP microdomains on the 0.1 μm size scale.[26] This still requires prolonged annealing times and care must be taken to prevent void formation when the CO_2 is removed. Ryu and co-workers reported that polystyrene-*b*-poly(methyl methacrylate) (PS-*b*-PMMA) lamellae with large periods are obtained by solvent annealing sequentially combined with thermal annealing, but this requires multiple steps.[27] In the development of BCPs for photonic bandgap applications, Thomas and co-workers used conventional BCPs and polyelectrolyte-based BCP with solvents or homopolymer/small molecule

* Address correspondence to russell@mail.pse.umass.edu, rhg@caltech.edu.

Received for review May 24, 2013 and accepted October 24, 2013.

Published online October 24, 2013
10.1021/nn402639g

additives to achieve periodicities on the scale of 100 nm and larger.[28−30] However, to achieve highly ordered structures on the 0.25 μm size scale or larger in an easy, rapid manner with BCPs has been exceedingly difficult.

Brush polymers consist of a linear polymer chain with polymer side chains densely attached to the main backbone chain.[31−34] Due to steric hindrance between the densely grafted brush side chains, brush polymers have an extended backbone configuration and a reduced number of backbone chain entanglements, in comparison to conventional, linear polymers with the same MW. Rheological studies of McKenna and Grubbs indicate that the brush polymers are, in fact, disentangled.[35] Up to now, there have been relatively few efforts to fabricate and control the ordering and orientation of periodic nanostructures using these unusual molecules.[36,37]

Numerous researchers have proposed different routes to synthesize brush polymers, but drawbacks, including a variety of issues associated with the efficiency of initiation of macroinitiators, high degrees of conversion of monomers, purification of unreacted brush side chains, synthesis procedures, and targeted MW and polydispersity index (PDI), have frequently been reported.[37−42] Recently, Grubbs and co-workers reported a novel ring-opening metathesis polymerization (ROMP) exploiting the high ring strain of norbornene monomer and the high activity of Ru-based olefin metathesis catalyst to synthesize brush block copolymers (brush BCPs) and brush random copolymers with ultrahigh MW, narrow PDI, and well-defined, structural architectures.[31] Recently, it is reported that brush BCPs self-assemble rapidly upon thermal annealing due to a reduced number of entanglements between brush BCPs, and the domain spacing dependence on backbone length was determined to be approximately linear.[43] Periodic nanostructures with large feature sizes in the bulk were reported, but well-developed nanopatterns with large feature sizes from brush polymers to prepare templates and scaffolds for various practical applications mentioned above have not yet been achieved.

Here, we present a simple route to generate two-dimensional, highly ordered, periodic nanopatterns with large feature sizes, using the self-assembly of brush block copolymers (brush BCPs). We also report the scaling relationship between the MW of brush polymers and the domain spacing observed from the self-assembled brush polymers.

RESULTS AND DISCUSSION

Table 1 shows the sample codes and characteristics of the brush BCPs used in this study. ω-Norbornenyl macromonomers containing polystyrene (PS) and polylactide (PLA) were synthesized and used to prepare the brush BCPs according to the previously reported procedure.[31,44] In the sample code form $[g\text{-}S_x]_p\text{-}b\text{-}[g\text{-}LA_y]_q$, the subscripts x and y are the molecular weights of side chains of each type (in units of one thousand), and subscripts p and q represent the degree of polymerization of each brush block. Thin films of brush BCPs were prepared on silicon substrates and, to effectively induce well-developed nanostructures, thin films were then solvent-annealed using either pure tetrahydrofuran (THF) or a mixture of solvents, tetrahydrofuran and chlorobenzene (THF/CBz), by which interfacial interactions were mediated. Scanning force microscopy (SFM), transmission electron microscopy (TEM), grazing incidence small-angle X-ray scattering (GI-SAXS), and grazing incidence wide-angle X-ray scattering (GI-WAXS) were used to characterize thin films of the brush BCPs.

TABLE 1. Sample Codes and Characteristics of Brush Polymers

	MW[a] of			DP[e] of			
sample codes	*g*-S[b]	*g*-LA[c]	total MW[d]	[*g*-S]	[*g*-LA]	total DP	L^f (nm)
$[g\text{-}S_{2.4}]_{19}\text{-}b\text{-}[g\text{-}LA_{2.4}]_{25}$	2.4k	2.4k	105k	19	25	44	22.0
$[g\text{-}S_{2.4}]_{35}\text{-}b\text{-}[g\text{-}LA_{2.4}]_{43}$			186k	35	43	78	40.0
$[g\text{-}S_{2.4}]_{51}\text{-}b\text{-}[g\text{-}LA_{2.4}]_{67}$			281k	51	67	118	61.0
$[g\text{-}S_{2.4}]_{98}\text{-}b\text{-}[g\text{-}LA_{2.4}]_{124}$			529k	98	124	222	116.0
$[g\text{-}S_{2.4}]_{189}\text{-}b\text{-}[g\text{-}LA_{2.4}]_{233}$			1007k	189	233	422	215.1
$[g\text{-}S_{2.4}]_{259}\text{-}b\text{-}[g\text{-}LA_{2.4}]_{381}$			1525k	259	381	640	[g]
$[g\text{-}S_{4.3}]_{11}\text{-}b\text{-}[g\text{-}LA_{4.5}]_{14}$	4.3k	4.5k	104k	11	14	25	20.9
$[g\text{-}S_{4.3}]_{19}\text{-}b\text{-}[g\text{-}LA_{4.5}]_{25}$			192k	19	25	44	31.1
$[g\text{-}S_{4.3}]_{32}\text{-}b\text{-}[g\text{-}LA_{4.5}]_{42}$			320k	32	42	74	45.2
$[g\text{-}S_{4.3}]_{42}\text{-}b\text{-}[g\text{-}LA_{4.5}]_{58}$			432k	42	58	100	62.2
$[g\text{-}S_{4.3}]_{93}\text{-}b\text{-}[g\text{-}LA_{4.5}]_{128}$			954k	93	128	221	149.5
$[g\text{-}S_{4.3}]_{206}\text{-}b\text{-}[g\text{-}LA_{4.5}]_{278}$			2089k	206	278	484	[g]
$[g\text{-}S_{4.8}]_{35}\text{-}b\text{-}[g\text{-}LA_{5.6}]_{18}$	4.8k	5.6k	271k	35	18	53	36[h]
$[g\text{-}S_{4.8}]_{66}\text{-}b\text{-}[g\text{-}LA_{5.6}]_{36}$			518k	66	36	102	67[h]
$[g\text{-}S_{5.1}]_{54}\text{-}b\text{-}[g\text{-}LA_{4.4}]_{51}$	5.1k	4.4k	500k	54	51	105	60.1
$[g\text{-}S_{6.1}]_{24}\text{-}b\text{-}[g\text{-}LA_{6.3}]_{31}$	6.1k	6.3k	326k	24	31	55	38.5[h]
$[g\text{-}S_{6.1}]_{40}\text{-}b\text{-}[g\text{-}LA_{6.3}]_{57}$			574k	40	57	97	56[h]

[a] Molecular weight determined by comparing the integrations of the norbornenyl olefin and polymer backbone signals from ^{1}H NMR spectra in $CDCl_3$. [b] Macromonomer of polystyrene. [c] Macromonomer of polylactide. [d] Molecular weight determined by THF GPC using RI and MALLS detector. [e] Degree of polymerization determined by ^{1}H NMR and THF GPC. [f] Center-to-center distance between microdomains determined by GI-SAXS analysis. [g] Microdomains spacing was not available by GI-SAXS analysis. [h] Center-to-center distance between microdomains determined by SFM image analysis.

Vayer *et al.* previously reported that the microdomains of PS-*b*-PLA were oriented normal to the substrate upon solvent annealing with CBz.[45] However, when thin films of $[g\text{-}S_{5.1}]_{54}\text{-}b\text{-}[g\text{-}LA_{4.4}]_{51}$, with a thickness of 40.7 nm, were solvent-annealed with pure CBz, no clear microphase separation and no significant morphological changes before or after solvent annealing were observed, even after prolonged annealing times (data not shown). From calculations of the polymer−solvent interaction parameters,[45] $\chi_{PS\text{-}CBz}$ and $\chi_{PLA\text{-}CBz}$ were determined to be 0.01 and 1.21 at 25 °C, respectively, which suggests that chain mobility arising from the solubilization of the polymers was insufficient to develop highly ordered periodic structures due to the

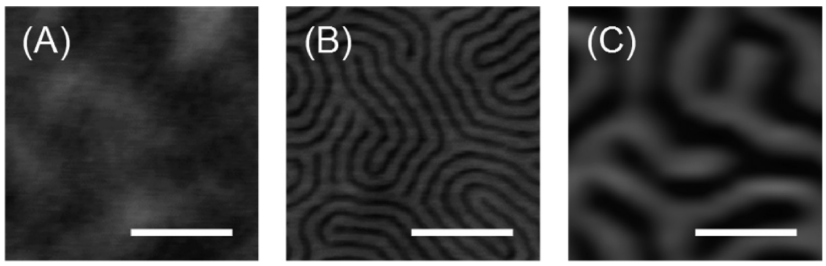

Figure 1. SFM (A, B) height images of solvent annealed thin films of $[g\text{-}S_{5.1}]_{54}$-*b*-$[g\text{-}LA_{4.4}]_{51}$ on Si substrate and SFM (C) height image of solvent-annealed thin films of $[g\text{-}S_{2.4}]_{189}$-*b*-$[g\text{-}LA_{2.4}]_{233}$ on Si substrate. The solvent-annealing times are 0 h for (A), 4 h for (B), and 10 h for (C). The scale bars in (A−C) are 400 nm.

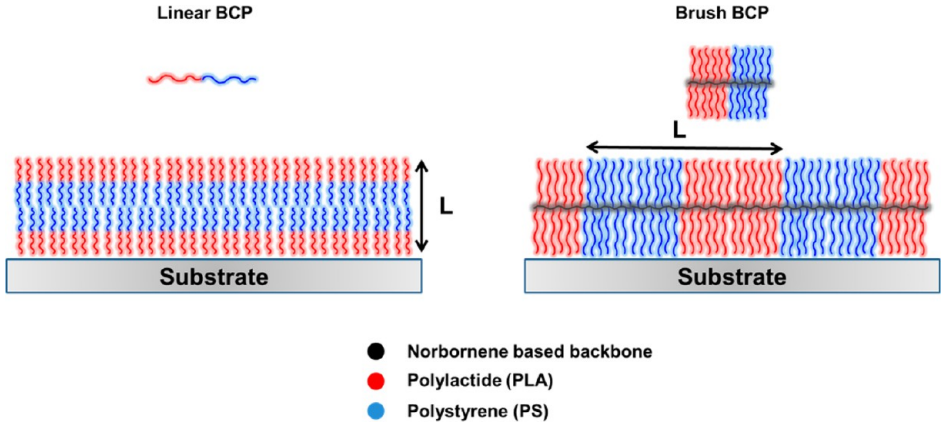

Scheme 1. Schematic of lamellar microdomains oriented parallel (left) or perpendicular (right) to the substrate from the self-assembly of a linear BCP or brush BCP.

poor solubility of PLA in CBz and the high MW of $[g\text{-}S_{5.1}]_{54}$-*b*-$[g\text{-}LA_{4.4}]_{51}$. In addition, Vayer *et al.* used cylinder forming PS-*b*-PLA, where PS was the major component. The results suggested that cylinder forming PS-*b*-PLA had higher chain mobility than the lamellar forming $[g\text{-}S_{5.1}]_{54}$-*b*-$[g\text{-}LA_{4.4}]_{51}$ used in our experiments, when annealed with only CBz. Therefore, mixed solvents of THF/CBz, where the increased attractive interaction between the cosolvents, THF and PLA, imparts enhanced mobility to the brush BCPs, were used to anneal the thin films of the lamellar forming $[g\text{-}S_{5.1}]_{54}$-*b*-$[g\text{-}LA_{4.4}]_{51}$ ($\chi_{PS\text{-}THF}$ and $\chi_{PLA\text{-}THF}$ were determined to be 0.15 and 0.62,[45] respectively). Solvent annealing in pure THF vapor was also used, and found to be suitable to promote the ordering of the brush BCPs.

Figure 1 shows that microphase separation was found through the entire film, while the mixed solvent annealing and well-developed lamellar microdomains, oriented normal to the surface, formed after solvent annealing. The center-to-center distance between lamellar microdomains or periodicity (*L*) of $[g\text{-}S_{5.1}]_{54}$-*b*-$[g\text{-}LA_{4.4}]_{51}$ was found to be 65.0 nm from the data in Figure 1B, and the step height between the [*g*-S] microdomain and the [*g*-LA] microdomain was found to be 2.4 nm from the height profile in Figure 1B (see Supporting Information), which arises from the difference in the solubilities of the block with the solvent. These data show that the surface is flat without significant surface roughness (see Supporting Information). Interestingly, when thin films of $[g\text{-}S_{2.4}]_{189}$-*b*-$[g\text{-}LA_{2.4}]_{233}$ (film thickness was measured to be 47 nm by ellipsometry), which has an extremely high MW of 1007k, were solvent-annealed with THF/CBz, well-developed lamellar microdomains oriented perpendicular to the substrate were also obtained within a relatively short solvent-annealing time, as shown in Figure 1C. From the SFM analysis, *L* of $[g\text{-}S_{2.4}]_{189}$-*b*-$[g\text{-}LA_{2.4}]_{233}$ is measured to be 228.5 nm. Again, the microphase separation of the brush BCP is rapid, in comparison to conventional BCPs. This is due to the fact that the brush BCP backbone is more rigid than that of a conventional flexible BCP caused by steric hindrance and, consequently, there is a reduction in the number of chain-entanglements when compared to analogous linear BCPs with the same MW. Therefore, even ultrahigh MW brush BCPs will rapidly self-assemble into well-ordered microphase-separated morphologies having extremely large feature sizes. Additional SFM images of lamellar-forming $[g\text{-}S_{2.4}]_p$-*b*-$[g\text{-}LA_{2.4}]_q$ and $[g\text{-}S_{4.3}]_p$-*b*-$[g\text{-}LA_{4.5}]_q$ series are given in the Supporting Information. It was also remarkable that lamellar microdomains formed by those brush BCPs were oriented perpendicular to the substrate without any need of surface modification. As shown in Scheme 1, the conventional linear BCPs will generally form a layer-by-layer structure due to the surface energy difference between two blocks and preferential interactions between one

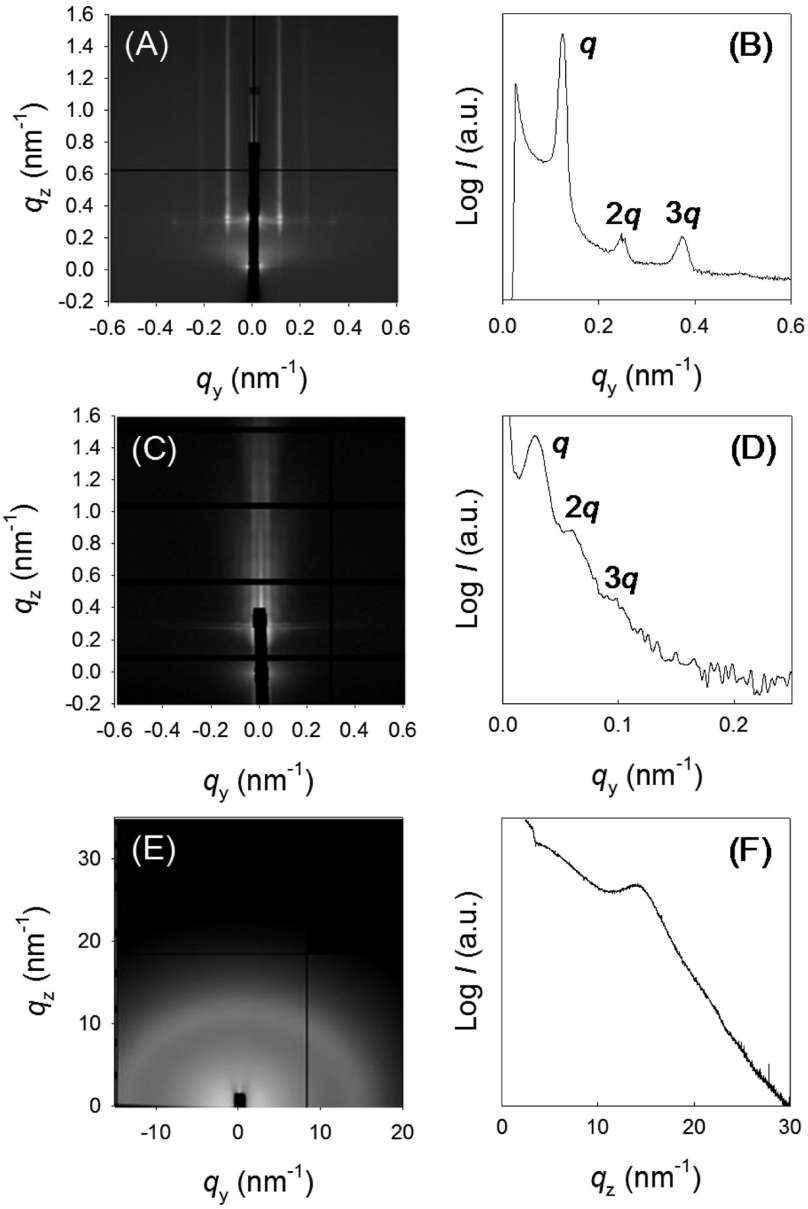

Figure 2. GI-SAXS patterns of thin films of (A) $[g\text{-}S_{5.1}]_{54}$-b-$[g\text{-}LA_{4.4}]_{51}$ and (C) $[g\text{-}S_{2.4}]_{189}$-b-$[g\text{-}LA_{2.4}]_{233}$ on Si substrates, where (A) and (C) are corresponding to the samples in Figure 1C and E, respectively. GI-WAXS pattern of thin films of (E) $[g\text{-}S_{5.1}]_{54}$-b-$[g\text{-}LA_{4.4}]_{51}$ on Si substrate, where (E) is corresponding to the sample in Figure 1C. The line profiles of scattering as a function of the scattering vector in (B), (D), and (F) are corresponding to (A), (C), and (E). q_y is the in-plane scattering vector and q_z is the out-of-plane scattering vector.

block and the substrate or air interface. However, for the brush BCPs used in this study, lamellar microdomains were oriented perpendicular to the substrate, the origin of which was attributed to the entropy gain caused by the unique chain architecture.

The fact that no special steps were taken to modify the substrate to control interfacial interactions,[46−49] and the orientation of the lamellar microdomains normal to the substrate, even with solvent annealing, was surprising, because PLA has strongly preferential interactions with the oxide layer on the silicon substrate, and the orientation found requires that the PS block be in contact with the substrate. Consequently, the orientation of the lamellar microdomains normal to the substrate may arise from the screening of the interactions of the blocks with the substrate, coupled with the more favored parallel alignment of the sterically hindered, rigid blocks at the substrate and from increasing the number of chain ends at the polymer/substrate interface, which again is an entropic-type of preferred chain orientation. Unlike linear BCPs, the many chain ends of the side chains attached to the backbone would preferentially segregate to the surface and substrate interfaces. This orientation allows the microphase-separated brush BCPs to have more conformational degrees of freedom, in comparison to the case where microdomains of brush BCPs are oriented parallel to the substrate.

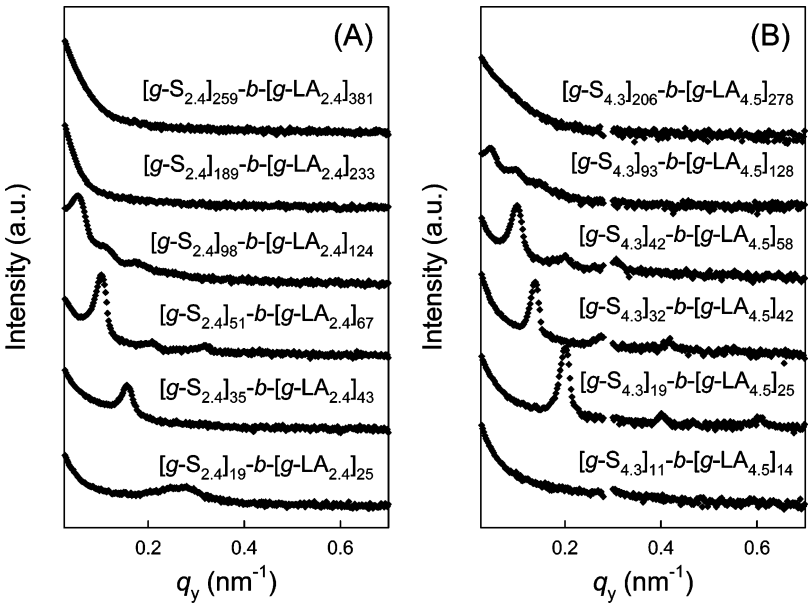

Figure 3. GI-SAXS patterns from Brush BCP thin films having different side chains: (A) MW of PS side chain is 2.4k and MW of PLA side chain is 2.4k; (B) MW of PS side chain is 4.3k and MW of PLA side chain is 4.5k (Thickness data for each series can be found in Supporting Information).

GI-SAXS was performed to analyze the structure of brush BCP thin films. The incidence angle was fixed at 0.18°, which is above the critical angle of the brush BCPs but below that of Si substrate, so that the X-ray beam penetrates into the polymer film. Figure 2A–D shows the GI-SAXS patterns and the line scans along the horizon of the GI-SAXS patterns of the thin films of $[g\text{-}S_{5.1}]_{54}$-*b*-$[g\text{-}LA_{4.4}]_{51}$ and $[g\text{-}S_{2.4}]_{189}$-*b*-$[g\text{-}LA_{2.4}]_{233}$ corresponding to the samples in Figure 1B and C, respectively. Upon solvent annealing, Bragg rods were observed at scattering vectors with magnitudes of $n(L/2\pi)$, where n is an integer, as shown in Figure 2A for $[g\text{-}S_{5.1}]_{54}$-*b*-$[g\text{-}LA_{4.4}]_{51}$ and Figure 2C for $[g\text{-}S_{2.4}]_{189}$-*b*-$[g\text{-}LA_{2.4}]_{233}$. Figure 2B and D show the one-dimensional profile of Figure 2A and C along q_y (in the plane of the film), respectively, where multiple orders of scattering were seen from the well-developed lamellar microdomains oriented perpendicular to the substrate. From the first scattering vector, L, for $[g\text{-}S_{5.1}]_{54}$-*b*-$[g\text{-}LA_{4.4}]_{51}$ and $[g\text{-}S_{2.4}]_{189}$-*b*-$[g\text{-}LA_{2.4}]_{233}$ was calculated to be 60.1 and 215.1 nm, respectively, which is consistent with L obtained from SFM images. Grazing-incidence wide-angle X-ray scattering (GI-WAXS) was also used to characterize thin brush BCP films. Figure 2E shows a clear ring of scattering, characteristic of a disordered, amorphous polymer with a maximum scattering peak corresponding to 0.43 nm. This distance arises from the average separation distance between adjacent brush side chains and, due to the lack of orientation in the GI-WAXS pattern, these data indicate that brush side chains are randomly distributed within the microdomains. The GI-SAXS studies on the two series of brush BCPs, $[g\text{-}S_{2.4}]_p$-*b*-$[g\text{-}LA_{2.4}]_q$ and $[g\text{-}S_{5.1}]_p$-*b*-$[g\text{-}LA_{4.4}]_q$, are shown in Figure 3. From the first order reflection in the GI-SAXS, the

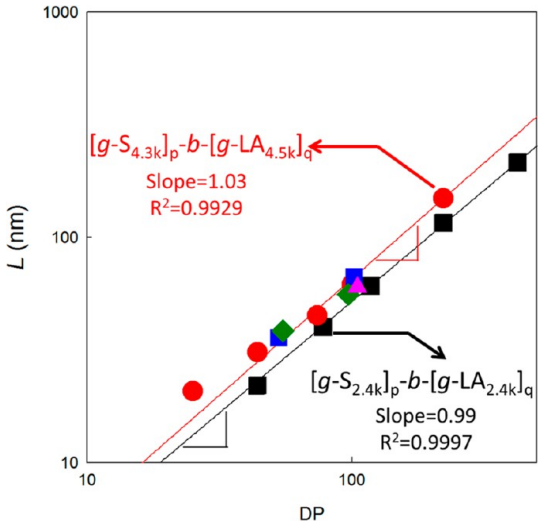

Figure 4. Plot of the period (L) as a function of degree of polymerization (DP) of the backbone for brush BCPs with different side chains (2.5k for S and 2.5k for LA (black square), 4.3k for S and 4.5k for LA (red circle), 4.8k for S and 5.6k for LA (blue square), 5.1k for S and 4.4k for LA (pink triangle), and 6.1k for S and 6.3k for LA (green diamond)).

period, L, was determined. Figure 4 shows L as a function of DP (degree of polymerization) for both series of brush BCPs (results are summarized in Table 1). From a regression analysis of the data, it was found that $L \propto DP^{0.99}$ for the $[g\text{-}S_{2.4}]_p$-*b*-$[g\text{-}LA_{2.4}]_q$ brush BCPs and $L \propto DP^{1.03}$ for the $[g\text{-}S_{4.3}]_p$-*b*-$[g\text{-}LA_{4.5}]_q$ brush BCPs. The slight increase in the exponent as the side chain length increases, and the apparent saturation, with a further increase in the side chain molecular weight, arises from the entropic penalty associated with the packing of the side chains. It is evident, though, that the backbone

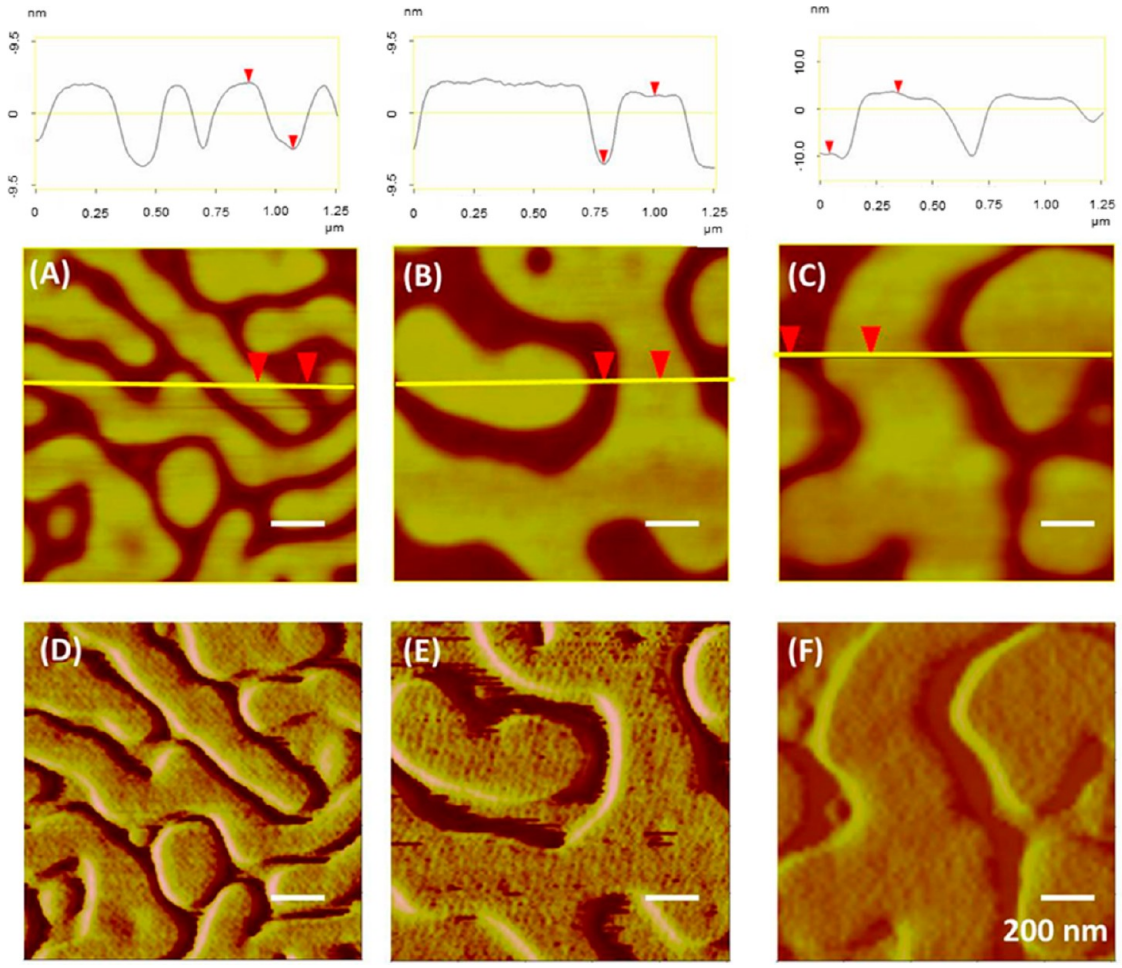

Figure 5. SFM height (A−C) and phase (D−F) images obtained from thin films of $[g\text{-}S_{2.4}]_{189}$-*b*-$[g\text{-}LA_{2.4}]_{233}$, $[g\text{-}S_{2.4}]_{259}$-*b*-$[g\text{-}LA_{2.4}]_{381}$, and $[g\text{-}S_{4.3}]_{206}$-*b*-$[g\text{-}LA_{4.5}]_{278}$ on Si substrates, respectively. The plots above SFM images were cross sectional analysis of the corresponding height images below.

chain is highly stretched, regardless of MW of the side chain, and only the extended contour length of the main chain dictates *L*. It should be noted that the exponent for the brush BCPs is much larger than that for flexible BCPs in the strong segregation regime,[16] where $L \propto DP^{2/3}$. Previously, we found similar results in case of thermally annealed bulk samples of brush BCPs.[43] In particular, the domain spacing found with solvent annealing is consistently larger than that for thermal annealing, because the swollen domain spacing during solvent annealing is kinetically trapped during the evaporation of the solvent vapor after the sample is removed from the annealing jar. Consequently, the exponents in the bulk state (thermal annealing) are smaller than that in film state (solvent annealing), indicating that the backbone chains are more stretched in solvent-annealed films. Brush BCPs with even larger side chain MW (5.0k and 6.0k) are also shown in Figure 4 and Table 1. The results for these are in keeping with the data for $[g\text{-}S_{4.3}]_p$-*b*-$[g\text{-}LA_{4.5}]_q$.

Thin films made from the highest MW brush BCPs showed a very curious surface topography after solvent annealing for 2 h in THF vapor. The film thickness in Figure 5A−C was determined by ellipsometry to be 60, 63, and 65 nm, respectively. A uniform height difference between the two microdomains was observed in Figure 5A and B, where representative thin films of brush BCPs with the same side chain MWs but with different DPs of the backbone ($[g\text{-}S_{2.4}]_{189}$-*b*-$[g\text{-}LA_{2.4}]_{233}$ and $[g\text{-}S_{2.4}]_{259}$-*b*-$[g\text{-}LA_{2.4}]_{381}$) were shown. Analysis of the surface topography shows that terraces formed on the surface with a step height of only 9 nm for both brush BCPs. This is far less than the step height, *L*, arising from incommensurability between the film thickness and *L*, when the microdomains orient parallel to the surface.[50,51] When the molecular weight of the side chains was increased, as shown in Figure 5C ($[g\text{-}S_{4.3}]_{206}$-*b*-$[g\text{-}LA_{4.5}]_{278}$), the step changed to being 13 nm. These values correspond roughly to the diameters of the brushes and suggest that there is a single layer of the brush BCP covering the surface of the film. X-ray photon spectroscopy (XPS) was used to characterize the composition of the surface of the films (see Supporting Information), which, from an atomic concentration analysis, suggests that the PS-brush block is preferentially covering the surface. This would be consistent with the lower surface energy of the PS-brush block, but also suggests that the

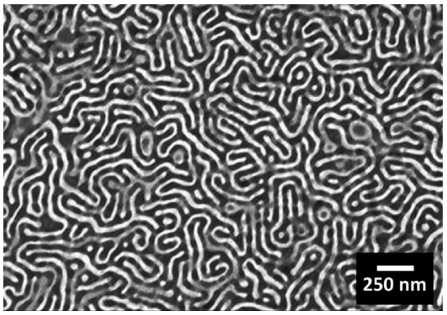

Figure 6. TEM images of solvent-annealed thin film of [*g*-$S_{5.1}$]$_{54}$-*b*-[*g*-$LA_{4.4}$]$_{51}$ after selective etching of PLA domains by hydrolysis under basic condition.

brush BCP must assume a rather unusual, bent configuration at the surface in order to minimize the surface energy. The exact nature of this configuration is unknown, at present, and is under further study. It is also noted that the difference in film thickness and solvent annealing time can have a significant influence on final morphologies; for example, both Figure 1C and Figure 5A are from the same sample, but behave differently.

It was previously reported that porous templates and scaffolds can be prepared from thin films of BCPs based on PS and PLA, by selectively hydrolyzing the PLA with a weak acid or weak base.[45] A thin film of [*g*-$S_{5.1}$]$_{54}$-*b*-[*g*-$LA_{4.4}$]$_{51}$, after solvent annealing with THF/CBz, was immersed into an aqueous sodium hydroxide (NaOH) basic solution to selectively remove the PLA domains. From the transmission electron microscopy (TEM) image in Figure 6, it was seen that the framework of the lamellar domains oriented normal to the substrate was preserved after hydrolysis, with trenches extending from the surface to the substrate. These porous templates can be used for transferring the original lamellar pattern, into either hard or flexible substrates, by reactive ion etching protocols in a very simple, routine manner. It is also expected that removal of one of the blocks and backfilling with other materials, such as a metal, could afford a simple route in producing *meta*-materials. It must be kept in mind that the brush polymers block has remained unaltered during the removal of the BrPLA block and, hence, lift-off or mask removal can be done by rinsing with a solvent of the brush polymers block. These templates and scaffolds achieved by brush BCPs can be used for practical applications like polarizers when these line patterns can be aligned through the directed self-assembly procedure.

CONCLUSIONS

In summary, we have demonstrated a simple route to fabricate two dimensionally well-ordered, periodic nanopatterns using brush BCPs, which generates structures with feature sizes on the tenths of a micrometer size scale in a relatively short time, owing to the reduced entanglements of the brush BCP chains. The scaling law was determined to be linear for the period, *L*, as a function of backbone degree of polymerization. It is evident that the backbone chain is highly stretched, regardless of the MW of the side chain, and only the extended contour length of the main chain dictates *L*. By a simple hydrolysis, these thin brush BCP films can be used as templates and scaffolds for pattern transfer or backfilling processes to generate inorganic structures on either hard or flexible surfaces (that may or may not be transparent). This strategy is ideal for the fabrication of polarizers and photonic band gap materials for visible, ultraviolet, and even infrared lights. An unusual terracing on the surface of the brush BCPs films was observed where layers of the lower surface energy block, one molecular diameter in thickness, were present on the surface, so as to reduce the surface energy of the films. The molecular configuration necessary to achieve this terracing is still under investigation.

EXPERIMENTAL SECTION

Brush BCPs were synthesized according to the previously reported procedure.[31,44] The Si substrate was cleaned with a carbon dioxide CO_2 snow jet and followed by oxygen plasma treatment for 10 min. Thin films of brush BCPs were prepared by spin-coating the solutions of brush BCPs and chlorobenzene on Si substrates, where the film thickness was controlled by adjusting the concentration of solution and the speed of spin coating. Solvent annealing was performed at room temperature and humidity of 30−40%: (i) thin film of BCP was placed in a closed cylindrical container (volume ∼ 250 mL) for solvent annealing after purging the jar with dry N_2 gas; (ii) solvent with an amount of 200 to 800 μL was added by a syringe into the closed container through a hole without opening the jar, and solvent annealing was performed in the container to prepare well-developed nanostructures. When the solvent annealing was done, the sample was immediately taken out from the jar and was dried at room temperature. The schematic process of solvent annealing can be found in Supporting Information. The surface topographies of brush BCPs thin films on Si substrates were imaged by the SFM (Digital Instruments, Nanoscope III) in tapping mode. Grazing Incidence Small Angle X-ray Scattering (GI-SAXS) measurements or Grazing Incidence Wide Angle X-ray Scattering (GI-WAXS) measurements were performed on beamline 7.3.3 at the Advanced Light Source at the Lawrence Berkeley National Laboratory. The wavelength of X-rays used was 1.24 Å, and the scattered intensity was detected using a 2D charge-coupled device (CCD) camera or a Pilatus 100k fast detector. Bright-field TEM was performed on a JEOL-2000FX TEM operating at an accelerating volatge of 200 kV. XPS survey spectra were recorded using a Physical Electronics Quantum 2000 spectrometer with a 200 μm spot size, monochromatic Mg Kα excitation, and a takeoff angle of 15 and 75°. The sensitivity factors specified for the spectromenter were used for quantitative analysis.

Conflict of Interest: The authors declare no competing financial interest.

Supporting Information Available: SFM images, XPS survey spectra, and GI-SAXS patterns are available. This material is available free of charge *via* the Internet at http://pubs.acs.org.

Acknowledgment. This work was supported by the U.S. Department of Energy (DOE), Office of Basic Energy Sciences

under contract DEFG02-96ER45612 (SWH, WG and GJ were partially supported through DEFG02-96ER45612 and performed the samples preparation and x-ray scattering measurements under the guidance of TPR). BRS, supported by the Dow-Resnick Bridge award and the NSF (CHE-1048404), performed the synthesis of the materials under the guidance of RHG. JH, supported through Samsung Display, performed the theoretical calculations. We thank D. H. Lee and X. Gu for assistance with the GI-SAXS and GI-WAXS measurements; we thank W. Zhao for assistance with the TEM measurements. We thank Y. Xia for useful discussions on the synthesis of the brush BCPs. Use of the Advanced Light Source at the Lawrence Berkeley National Laboratory is acknowledged. The Advanced Light Source is supported by the Director, Office of Science, Office of Basic Energy Sciences, Material Science Division of the U.S. Department of Energy under Contract No. DE-AC02-05CH11231 at Lawrence Berkeley National Laboratory.

REFERENCES AND NOTES

1. Park, M.; Harrison, C.; Chaikin, P. M.; Register, R. A.; Adamson, D. H. Block Copolymer Lithography: Periodic Arrays of $\sim 10^{11}$ Holes in 1 Square Centimeter. *Science* **1997**, *276*, 1401–1404.
2. Li, R. R.; Dapkus, P. D.; Thompson, M. E.; Jeong, W. G.; Harrison, C.; Chaikin, P. M.; Register, R. A.; Adamson, D. H. Dense Arrays of Ordered GaAs Nanostructures by Selective Area Growth on Substrates Patterned by Block Copolymer Lithography. *Appl. Phys. Lett.* **2000**, *76*, 1689–1691.
3. Thurn-Albrecht, T.; Schotter, J.; Kästle, G. A.; Emley, N.; Shibauchi, T.; Krusin-Elbaum, L.; Guarini, K.; Black, C. T.; Tuominen, M. T.; Russell, T. P. Ultrahigh-Density Nanowire Arryas Grown in Self-Assembled Diblock Copolymer Templates. *Science* **2000**, *290*, 2126–2129.
4. Kim, H.-C.; Jia, X.; Stafford, C. M.; Kim, D. H.; McCarthy, T. J.; Tuominen, M.; Hawker, C. J.; Russell, T. P. A Route to Nanoscopic SiO_2 Posts *via* Block Copolymer Templates. *Adv. Mater.* **2001**, *13*, 795–797.
5. Cheng, J. Y.; Ross, C. A.; Chan, V. Z.-H.; Thomas, E. L.; Lammertink, R. G. H.; Vancso, G. J. Formation of a Cobalt Magnetic Dot Array *via* Block Copolymer Lithography. *Adv. Mater.* **2001**, *13*, 1174–1178.
6. Black, C. T.; Guarini, K. W.; Milkove, K. R.; Baker, S. M.; Russell, T. P.; Tuominen, M. T. Integration of Self-Assembled Diblock Copolymers for Semiconductor Capacitor Fabrication. *Appl. Phys. Lett.* **2001**, *79*, 409–411.
7. Lopes, W.; Jaeger, H. M. Hierarchical Self-Assembly of Metal Nanostructures on Diblock Copolymer Scaffolds. *Nature* **2001**, *414*, 735–738.
8. Black, C. T. Self-Aligned Self Assembly of Multi-Nanowire Silicon Field Effect Transistors. *Appl. Phys. Lett.* **2005**, *87*, 163116–1−3.
9. Pelletier, V.; Asakawa, K.; Wu, M.; Adamson, D. H.; Register, R. A.; Chaikin, P. M. Aluminum Nanowire Polarizing Grids: Fabrication and Analysis. *Appl. Phys. Lett.* **2006**, *88*, 211114–1−3.
10. Cheng, J. Y.; Ross, C. A.; Smith, H. I.; Thomas, E. L. Templated Self-Assembly of Block Copolymers: Top-Down Helps Bottom-Up. *Adv. Mater.* **2006**, *18*, 2505–2521.
11. Kang, Y.; Walish, J. J.; Gorishnyy, T.; Thomas, E. L. Broad-Wavelength-Range Chemically Tunable Block-Copolymer Photonic Gels. *Nat. Mater.* **2007**, *6*, 957–960.
12. Luttge, R. Massively Parallel Fabrication of Repetitive Nanostructures: Nanolithography for Nanoarrays. *J. Phys. D: Appl. Phys.* **2009**, *42*, 123001–1−18.
13. Xu, J.; Hong, S. W.; Gu, W.; Lee, K. Y.; Kuo, D. S.; Xiao, S.; Russell, T. P. Fabrication of Silicon Oxide Nanodots with an Areal Density Beyond 1 Teradots/Inch^2. *Adv. Mater.* **2011**, *22*, 5755–5760.
14. Hong, S. W.; Russell, T. P. In *Block Copolymer Thin Films: A Comprehensive Polymer Sciences*, 2nd ed.; Matyjaszewski, K., Möller, M., Eds.; Elsevier: Amsterdam, 2012; Vol. 7, pp 45−69.
15. Gu, X.; Liu, Z.; Gunkel, I.; Chourou, S. T.; Hong, S. W.; Olynick, D. L.; Russell, T. P. High Aspect Ratio sub-15 nm Silicon Trenches from Block Copolymer Templates. *Adv. Mater.* **2012**, *24*, 5688–5694.
16. Bates, F. S.; Fredrickson, G. H. Block Copolymer Thermodynamics: Theory and Experiment. *Annu. Rev. Phys. Chem.* **1990**, *41*, 525–557.
17. Hamley, I. W. Nanostruture Fabrication using Block Copolymers. *Nanotechnology* **2003**, *14*, R39–R54.
18. Park, C.; Yoon, J.; Thomas, E. L. Enabling Nanotechnology with Self Assembled Block Copolymer Patterns. *Polymer* **2003**, *44*, 6725–6760.
19. Segalman, R. A. Patterning with Block Copolymer Thin Films. *Mater. Sci. Eng., R* **2005**, *48*, 191–226.
20. Stoykovich, P.; Nealey, P. F. Block Copolymers and Conventional Lithography. *Mater. Today* **2006**, *9*, 20–29.
21. Park, S.; Lee, D. H.; Xu, J.; Kim, B.; Hong, S. W.; Jeong, U.; Xu, T.; Russell, T. P. Macroscopic 10-Terabit-per-Square-Inch Arrays from Block Copolymers with Lateral Order. *Science* **2009**, *323*, 1030–1033.
22. Marencic, A. P.; Register, R. A. Controlling Order in Block Copolymer Thin Films for Nanopatterning Applications. *Annu. Rev. Chem. Biomol. Eng.* **2010**, *1*, 277–297.
23. Albert, J. N. L.; Epps, T. H., III Self-Assembly of Block Copolymer Thin Films. *Mater. Today* **2010**, *13*, 24–33.
24. Tseng, Y.-C.; Darling, S. B. Block Copolymer Nanostructures for Technology. *Polymers* **2010**, *2*, 470–489.
25. Gedde, U. F. *Polymer Physics*; Springer: London, 1995.
26. Ramachandrarao, V. S.; Gupta, R. R.; Russell, T. P.; Watkins, J. J. Rapid Directed Assembly of Block Copolymer Films at Elevated Temperatures. *Macromolecules* **2001**, *34*, 7923–7925.
27. Kim, E.; Ahn, H.; Park, S.; Lee, M.; Lee, S.; Kim, T.; Kwak, E. A.; Lee, J. H.; Lei, X.; Huh, J.; *et al.* Directed Assembly of High Molecular Weight Block Copolymers: Highly Ordered Line Patterns of Perpendicularly Oriented Lamellae with Large Periods. *ACS Nano* **2013**, *7*, 1952–1960.
28. Fink, Y.; Urbas, A. M.; Bawendi, M. G.; Joannopoulos, J. D.; Thomas, E. L. Block Copolymers as Photonic Bandgap Materials. *J. Lightwave Technol.* **1999**, *17*, 1963–1969.
29. Kang, C.; Kim, E.; Baek, H.; Hwang, K.; Kwak, D.; Kang, Y.; Thomas, E. L. Full Color Stop Bands in Hybrid Organic/Inorganic Block Copolymer Photonic Gels by Swelling-Freezing. *J. Am. Chem. Soc.* **2009**, *131*, 7538–7539.
30. Yoon, J.; Mathers, R. T.; Coates, G. W.; Thomas, E. L. Optically Transparent and High Molecular Weight Polyolefin Block Copolymers Toward Self-Assembled Photonic Band Gap Materials. *Macromolecules* **2006**, *39*, 1913–1919.
31. Xia, Y.; Olsen, B. D.; Kornfield, J. A.; Grubbs, R. H. Efficient Synthesis of Narrowly Dispersed Brush Copolymers and Study of Their Assemblies: the Importance of Side Chain Arrangement. *J. Am. Chem. Soc.* **2009**, *131*, 18525–18532.
32. Saariaho, M.; Subbotin, A.; Szleifer, I.; Ikkala, O.; ten Brinke, G. Synthesis and Solubility of (Mono-) End-Functionalized Poly(2-hydroxyethyl methacrylate-*g*-ethylene glycol) Graft Copolymers with Varying Macromolecular Architectures. *Macromolecules* **1999**, *32*, 4439–4443.
33. Neugebauer, D.; Zhang, Y.; Pakula, T.; Matyjaszewski, K. PDMS-PEO Densely-Grafted Copolymers. *Macromolecules* **2005**, *38*, 8687–8693.
34. Neugebauer, D.; Theis, M.; Pakul, T.; Wegner, G.; Matyjaszewski, K. Densely-Heterografted Brush Macromolecules with Crystallizable Grafts. *Macromolecules* **2006**, *39*, 584–593.
35. Hu, M.; Xia, Y.; McKenna, G. B.; Kornfield, J. A.; Grubbs, R. H. Linear Rheological Response of a Series of Densely Branched Brush Polymers. *Macromolecules* **2011**, *44*, 6935–6943.
36. Runge, M. B.; Dutta, S.; Bowden, N. B. Synthesis of Comb Block Copolymers by ROMP, ATRP, and ROP and their Assembly in the Solid State. *Macromolecules* **2006**, *39*, 498–508.
37. Rzayev, J. Synthesis of polystyrene-polylactide Bottlebrush Block Copolymers and their Melt Self-Assembly into Large Domain Nanostructures. *Macromolecules* **2009**, *42*, 2135–2141.
38. Hadjichristidis, N.; Pitsikalis, M.; Iatrou, H.; Pispas, S. The Strength of the Macromonomer Strategy for Complex Macromolecular Architecture: Molecular Characterization,

Properties and Applications of Polymacromonomers. *Macromol. Rapid Commun.* **2003**, *24*, 979–1013.
39. Neugebauer, D.; Sumerlin, B. S.; Matyjaszewski, K.; Goodhart, B.; Sheiko, S. S. How Dense are Cylindrical Brushes Grafted from a Multifunctional Macroinitiator? *Polymer* **2004**, *45*, 8173–8179.
40. Schappacher, M.; Deffieux, A. From Combs to Comb-*g*-Comb Centipedes. *Macromolecules* **2005**, *38*, 7209–7213.
41. Gao, H.; Matyjaszewski, K. Synthesis of Molecular Brushes by "Grafting onto" Methods: Combination of ATRP and Click Reactions. *J. Am. Chem. Soc.* **2007**, *129*, 6633–6639.
42. Runge, M. B.; Bowden, N. B. Synthesis of High Molecular Weight Comb Block Copolymers and their Assembly into Ordered Morphologies in the Solid State. *J. Am. Chem. Soc.* **2007**, *129*, 10551–10560.
43. Gu, W.; Huh, J.; Hong, S. W.; Sveinbjornsson, B. R.; Park, C.; Grubbs, R. H.; Russell, T. P. Self-Assembly of Symmetric Brush Diblock Copolymers. *ACS Nano* **2013**, *7*, 2551–2558.
44. Sveinbjornsson, B. R.; Weitekamp, R. A.; Miyake, G. M.; Xia, Y.; Atwater, H. A.; Grubbs, R. H. Rapid Self-Assembly of Brush Block Copolymers to Photonic Crystals. *Proc. Natl. Acad. Sci. U.S.A.* **2012**, *109*, 14332–14336.
45. Vayer, M.; Hillmyer, M. A.; Dirany, M.; Thevenin, G.; Erre, R.; Sinturel, C. Perpendicular Orientation of Cylindrical Domains upon Solvent Annealing Thin Films of Polystyrene-*b*-polylactide. *Thin Solid Films* **2010**, *518*, 3710–3715.
46. Delamarche, E.; Michel, B.; Gerber, C.; Anselmetti, D.; Guentherodt, H. J.; Wolf, H.; Ringsdorf, H. Real-Space Observation of Nanoscale Molecular Domains in Self-Assembled Monolayers. *Langmuir* **1994**, *10*, 2869–2871.
47. Mansky, P.; Liu, Y.; Huang, E.; Russell, T. P.; Hawker, C. J. Controlling Polymer−Surface Interactions with Random Copolymer Brushes. *Science* **1997**, *275*, 1458–1460.
48. Ryu, D. Y.; Shin, K.; Drockenmuller, E.; Hawker, C. J.; Russell, T. P. A Generalized Approach to the Modification of Solid Surfaces. *Science* **2005**, *308*, 236–239.
49. Ji, S.; Liu, C. C.; Son, J. G.; Gotrik, K.; Craig, G. S. W.; Gopalan, P.; Himpsel, F. J.; Char, K.; Nealey, P. F. Generalization of the Use of Random Copolymers to Control the Wetting Behavior of Block Copolymer Films. *Macromolecules* **2008**, *41*, 9098–9103.
50. Russell, T. P.; Coulon, G.; Deline, V. R.; Miller, D. C. Characteristics of the Surface-Induced Orientation for Symmetric Diblock PS/PMMA Copolymers. *Macromolecules* **1989**, *22*, 4600–4606.
51. Anastasiadis, S. H.; Russell, T. P.; Satija, S. K.; Majkrzak, C. F. The Morphology of Symmetric Diblock Copolymers as Revealed by Neutron Reflectivity. *J. Chem. Phys.* **1990**, *92*, 5677–5691.